U·P·O·J

Mechanical Function of a Composite Nanofibrous Biomaterial Analogue of the Knee Meniscus Inclusive of Radial Inclusive of Radial Tie Fiber-Like Elements

Sonia Bansal, BS
Breanna Seiber, BS
Niobra Keah, MS
Robert Mauck, PhD
Miltiadis Zgonis, MD

Introduction

Menisci are semi-lunar shaped fibrocartilaginous wedges located between the femur and the tibial plateau and support the structure and mechanical function of the knee joint[1,2]. Understanding meniscus structure and function is particularly important given the high incidence of meniscal pathology[3,4]. Circumferentially aligned collagen bundles within the meniscus function to convert compressive forces into tensile hoop stresses[5,6]. In addition, the meniscus contains "radial tie fibers" that originate at the meniscus periphery and interdigitate amongst the circumferential fiber population[5-7]. These radial tie fibers (RTFs) vary in size, spatial distribution, and in their degree of arborization[7], and are thought to bind circumferential fibers together and protect against longitudinal splitting[8,9]. Radial tears interject perpendicularly and sever the circumferential bundles and are thought to compromise mechanical function, though recent studies demonstrated that reduction in load transfer occurs only when these tears reach 90% of the meniscus width[10].This suggests alternative methods for strain transmission in the meniscus. We hypothesize that RTFs play a role in this, particularly in the case of a radial tear. To further this line of inquiry, we quantified RTF density and size in adult menisci as a function of position, and measured the mechanical function of these tissue samples in the context of a radial tear. Additionally, we utilized electrospinning to generate a composite material model of the meniscus, with variable fiber mechanics in each layer, by spinning two polymers with distinct material characteristics.

Methods

Native Tissue Analysis

Medial menisci (n = 14) were harvested from adult (skeletally mature) cows. Six were divided into four equal regions: anterior horn, anterior body (Body-A), posterior body (Body-P), and posterior horn. Each region was cryosectioned in the sagittal plane to 10 μm thickness spanning the cross section and fixed. Three zones were examined: outer, middle, and inner zones. Sections were imaged at 10X via second harmonic generation (SHG, 840 nm excitation). Maximum projections (~5 microns thick) were generated in each zone and the area fraction with positive SHG signal computed as a measure of RTF area fraction (Figure 1A). Fiber thickness was estimated using the FIJI plugin BoneJ[11-13]. Metrics were compared across regions by ANOVA ($p \leq 0.05$) with Tukey's post-hoc tests; data are presented as the mean value for each region and zone (Fig. 1B,C).

Remaining menisci were trimmed as in Figure 2A to yield Anterior, Posterior, and Body segments. These were sectioned transversely into strips (5 × 15 x 0.3mm) with extended tabs for gripping[14]. Samples were preconditioned for 15 cycles (2%-4%) and then evaluated in tension in a ramp to 15% strain (0.5% strain/s). Post-testing, samples were re-equilibrated in PBS for 1 hr, defected with a 50% radial defect at the inner-zone, and retested as above to 50% strain. Stress versus strain data was curve-fit using a custom bilinear fitting program in MATLAB to define the 'toe' and 'linear' moduli[14,15]. Significance (n = 4/group) was analyzed using 1-way ANOVA ($p \leq 0.05$), with Tukey's post hoc; data are presented as mean ± SEM (Figure 2B,C).

Scaffold Fabrication and Mechanical Testing

Nanofibrous 75:25 poly(lactic-co-glycolic acid) (PLGA) and poly(ε-caprolactone) (PCL)

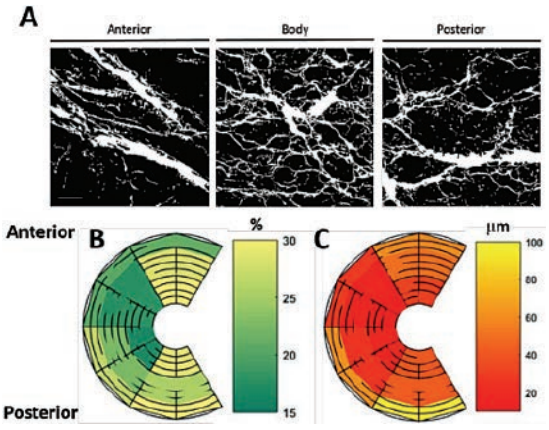

Figure 1. Radial tie fiber (RTF) distribution in adult menisci. **(A)** SHG images of the middle zone of each region, white shows positive SHG indicative of radial tie fiber presence (SB = 200 μm). **(B)** Radial tie fiber density, reported as Area Fraction (%) across the meniscus, and **(C)** Mean fiber thickness (μm).

Correspondence:
McKay Orthopaedic Laboratory
University of Pennsylvania
Philadelphia, PA
soslowsk@upenn.edu

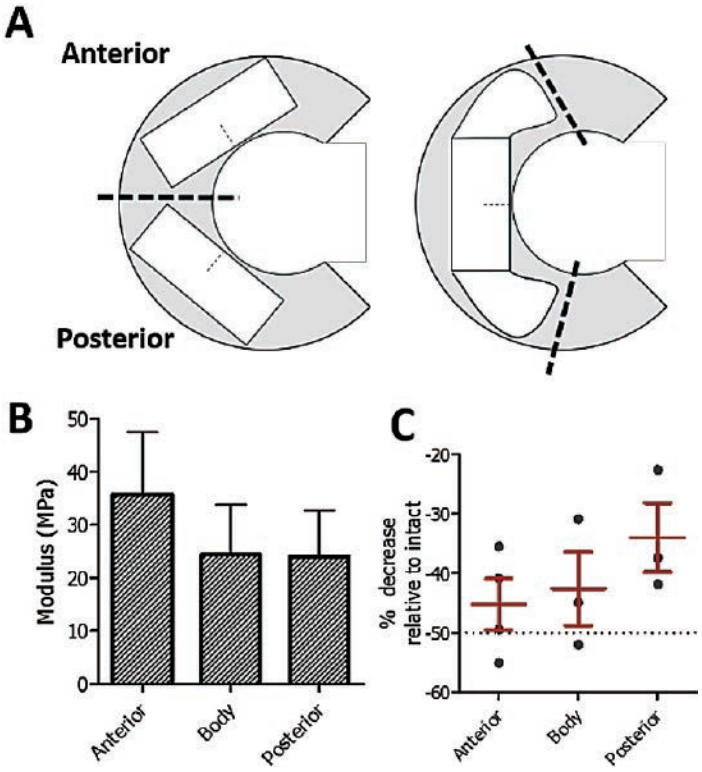

Figure 2. (A) Schematic of native tissue sample preparation **(B)** Linear moduli (LM) of intact tissues by location. **(C)** Change in LM of defected native tissue moduli measured prior to defect creation.

scaffolds were electrospun[7]. For aligned (AL) scaffolds, a mandrel rotating at 10 m/s served as the collector. To form non-aligned (NA) scaffolds, the mandrel was slowed to ~3 m/s. To replicate radial tie elements, AL scaffolds with discrete NA layers were produced by lowering the speed of the mandrel for set periods of time. Composite scaffolds had 7 alternating AL and NA layers (Figure 3A) with 33% distributed NA content overall. The composition of each layer was varied such that scaffolds with softer (PCL) or stiffer (PLGA) intervening NA layers were produced. Scaffolds were trimmed to 40 mm length (in the AL direction) × 5 mm width for testing. Two conditions were tested: intact or defect, with the latter having a radial cut spanning 50% of the width. Samples were evaluated in tension (ramp to 100% strain at 0.5% strain/s) (Figure 3B). Stress versus strain data was curve-fit as above and a custom MATLAB program used to determine the yield and failure strain and toughness. Significance (n = 6/group) was analyzed by 1-way ANOVA ($p \leq 0.05$), with Tukey's post hoc; data are presented as mean ± SEM (Figure 3C-F).

Results

SHG revealed differences in RTF fiber density between zones, with the central body lower than the anterior or posterior horns ($p < 0.05$). RTF thickness varied as a function of region ($p < 0.02$) and zone ($p < 0.005$) (Figure 1B,C). The linear modulus of anterior, body, and posterior sections (35.8 ± 11.8, 24.4 ± 9.5, and 24.0 ± 8.8 MPa) were not different from one another (p= 0.78). However, we noted an attenuation in the decrease in apparent modulus with defect of posterior samples compared to all other regions (Figure 2B,C).

For scaffolds, the linear region modulus of PLGA-only AL scaffolds was ~4x higher than PLGA NA scaffolds (241 ± 13 vs 53 ± 2 MPa, $p < 0.001$) and linear region moduli of AL and NA PLGA scaffolds were ~7 and ~5x higher than AL and NA PCL scaffolds, respectively (34 ± 2 and 11 ± 0 MPa, $p < 0.001$) (Figure 3C). Yield strains for AL and NA PLGA scaffolds (1.5 and 2.4%) were lower than PCL scaffolds (AL: 10% and NA: 6%, $p < 0.001$) (Fig. 3D). The greatest toughness of defected scaffolds was seen in AL PLGA scaffolds (1.1 ± .10 $J \cdot m^{-3} \cdot \mathbf{10}^{4}$, $p < 0.001$). Failure strain ranged from 36% (PLGA, AL) and 46% (PLGA, NA) in single-polymer scaffolds (Figure 3E,F).

Composite scaffolds showed distinct mechanical behavior

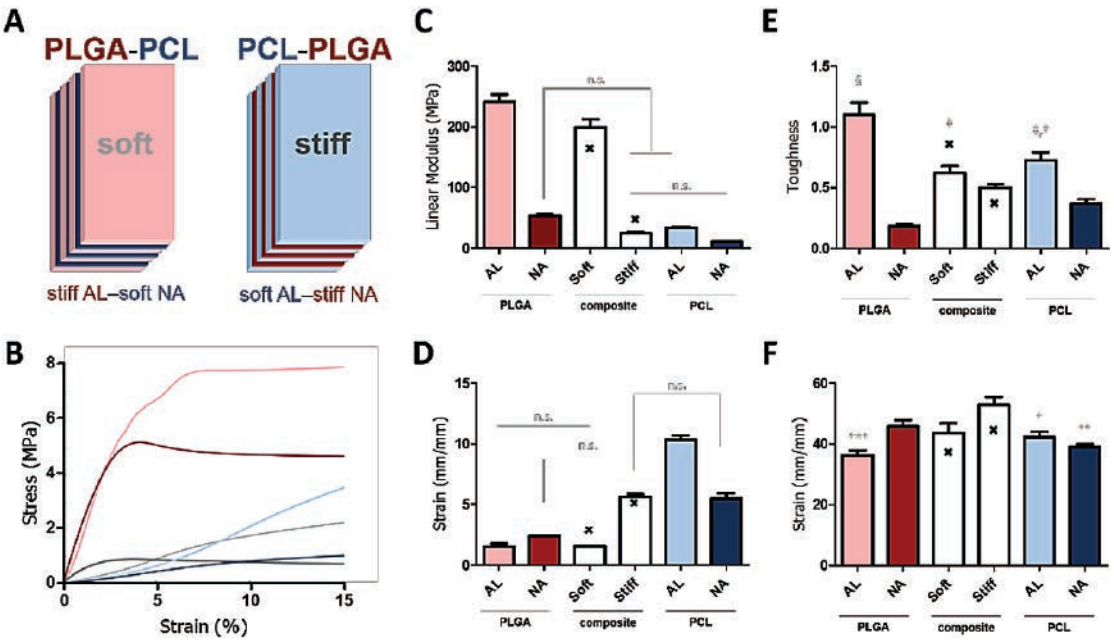

Figure 3. (A) Schematic of composite scaffold preparation **(B)** Stress-strain plots of each group to 15% strain. **(C)** Linear moduli and **(D)** yield strain of intact AL, NA, and composite scaffolds. $P > 0.01$unless otherwise indicated. **(E)** Toughness and **(F)** failure strain of defected AL, NA, and composite scaffolds, § = $p \leq 0.05$ vs. all other groups, Toughness. ‡ = $p \leq 0$ .01 vs. PLGA-NA, Toughness. † = $p \leq 0.01$ vs. PCL-NA, Toughness. * = $p \leq 0.05$ vs. PCL_PLGA, Failure strain. "x" indicates expected outcome from weighted mixture model.

that did not always match expectations, based on a simple weighted mixture model combining the individual components. Expected linear modulus of composites formed from AL PLGA with intervening NA PCL did not match predictions while the reverse configuration exceeded predicted value ($p = 0.0002$, Figure 3C). Toughness of AL PLGA/NA PCL scaffolds was lower than expected ($p = 0.01$) while AL PCL/NA PLGA scaffolds were higher than expected ($p = 0.008$) (Fig. 3D). Similarly, the yield strain of AL PLGA/NA PCL scaffolds was lower than expected values ($p < 0.0001$) while AL PCL/NA PLGA scaffolds were higher ($p = 0.04$) (Figure 3E). Conversely, strain at failure was under predicted for both, with this being significant for AL PCL/NA PLGA scaffolds ($p = 0.03$, Figure 3F).

Discussion

Radial tie fibers (RTFs) form a branched fiber network that interdigitates with circumferential fibers in the meniscus, and may function to stiffen the composite and make it more resistant to crack propagation. This effect would likely be contingent upon RTF density, distribution, and thickness. We found the greatest density of RTFs in the posterior horn, potentially reflecting the more demanding in vivo loading experienced in this region. Our finding of a trend towards a higher apparent modulus in the posterior horn (in the context of a radial defect) supports the hypothesis that RTFs play such a functional role. To study these interactions in a more controlled setting, we developed a biomaterial analog containing RTF-like elements. These distinct disorganized fibrous layers (that were interspersed in an otherwise aligned fiber array) altered scaffold mechanics. The finding of increased failure strain (compared to scaffolds of a single composition) supports the beneficial effects of RTF inclusion in native meniscus. This may act by enabling efficient and prolonged load transfer in the context of tears that interrupt the circumferential fibrous architecture. Understanding of this complex composite behavior will inform engineering design towards the fabrication of functional meniscus replacements, and could alter clinical practice with respect to surgical intervention.

Acknowledgements

This work was supported by the OREF New Investigator Grant, the NIH, and the VA.

References

1. Kambic HE, McDevitt CA. Spatial organization of types I and II collagen in the canine meniscus. *J Orthop Res,* 2005. Jan;23(1):142-9.

2. Chevrier A, Nelea M, Hurtig MB, Hoemann CD, Buschmann MD. *J Orthop Res,* 2009. Sep;27(9):1197-203. doi: 10.1002/jor.20869.

3. Merriam AR, Patel JM, Culp BM, Gatt CJ Jr, Dunn MG. Successful Total Meniscus Reconstruction Using a Novel Fiber-Reinforced Scaffold: A 16- and 32-Week Study in an Ovine Model. *Am J Sports Med,* 2015. Oct;43(10):2528-37. doi: 10.1177/0363546515595065. Epub 2015 Aug 21.

4. Mordecai SC, Al-Hadithy N, Ware HE, Gupte CM. Treatment of meniscal tears: an evidence based approach. *World J Orthop.* 2014. Jul 18;5(3):233-41. doi: 10.5312/wjo.v5.i3.233. eCollection 2014.

5. Skaggs DL, Warden WH, Mow VC. Radial tie fibers influence the tensile properties of the bovine medial meniscus. *J Orthop Res,* 1994. Mar;12(2):176-85.

6. Makris EA, Hadidi P, Athanasiou KA. The knee meniscus: structure-function, pathophysiology, current repair techniques, and prospects for regeneration. *Biomaterials,* 2011. Oct;32(30):7411-31. doi: 10.1016/j.biomaterials.2011.06.037. Epub 2011 Jul 18.

7. Andrews SH, Rattner JB, Abusara Z, Adesida A, Shrive NG, Ronsky JL. Tie-fibre structure and organization in the knee menisci. , *J Anat,* 2014. May;224(5):531-7. doi: 10.1111/joa.12170. Epub 2014 Mar 12.

8. Mauck RL, Baker BM, Nerurkar NL, Burdick JA, Li WJ, Tuan RS, Elliott DM. Engineering on the straight and narrow: the mechanics of nanofibrous assemblies for fiber-reinforced tissue regeneration. *Tissue Eng.* 2009. Part B Rev. 2009 Jun;15(2):171-93. doi: 10.1089/ten.TEB.2008.0652. Review.

9. Bullough PG, Munuera L, Murphy J, Weinstein AM. The strength of the menisci of the knee as it relates to their fine structure. *J Bone Joint Surgery,* 1970. Aug;52(3):564-7.

10. Bedi A, Kelly NH, Baad M, Fox AJ, Brophy RH, Warren RF, Maher SA. Dynamic contact mechanics of the medial meniscus as a function of radial tear, repair, and partial meniscectomy. *J Bone Joint Surg,* 2010. Jun;92(6):1398-408. doi: 10.2106/JBJS.I.00539.

11. Saalfeld, FIJI 2012.

12. Dougherty, FIJI 2006.

13. Schindelin J, Arganda-Carreras I, Frise E, Kaynig V, Longair M, Pietzsch T, Preibisch S, Rueden C, Saalfeld S, Schmid B, Tinevez JY, White DJ, Hartenstein V, Eliceiri K, Tomancak P, Cardona A. Fiji: an open-source platform for biological-image analysis. *Nat Methods,* 2012. Jun 28;9(7):676-82. doi: 10.1038/nmeth.2019.

14. Peloquin JM, Santare MH, Elliott DM. Advances in Quantification of Meniscus Tensile Mechanics Including Nonlinearity, Yield, and Failure. *J Biomech Eng, 2016.* Feb;138(2):021002. doi: 10.1115/1.4032354.

15. Tanaka ML, Weisenbach CA, Carl Miller M, Kuxhaus L. A continuous method to compute model parameters for soft biological materials. *J Biomech Eng,* 2011. Jul;133(7):074502. doi: 10.1115/1.4004412.